Article

Exploring Caffeic Acid and Lignosulfonate as Key Phenolic Ligands for Metal-Phenolic Network Assembly

Daniela Tomasetig,* Chenyu Wang, Nikolaus Hondl, Anton Friedl, and Hirotaka Ejima

Cite This: *ACS Omega* 2024, 9, 20444−20453

Read Online

ACCESS | Metrics & More | Article Recommendations | Supporting Information

ABSTRACT: Films formed by metals and phenols through a coordinative interaction have been extensively studied in previous years. We report the successful formation of MPN films from the phenolic compounds caffeic acid and lignosulfonate using Fe^{3+} ions for complexation. The likewise examined *p*-coumaryl alcohol showed some MPN film formation tendency, while for coniferyl alcohol and sinapyl alcohol, no successful film buildup could be observed. These newly formed films were compared to tannic acid-Fe^{3+} films as a reference. Film growth and degradation were tracked by using UV−vis absorption spectroscopy. The films were degradable under different conditions such as alkaline environments or in the presence of a strong chelator. Small hollow capsules with a diameter of 3 μm and thicknesses in the nanometer range were produced. Additionally, the prepared films showed varying colors and levels of wettability. By utilizing the films' coating properties, we successfully dyed human hair in various colors.
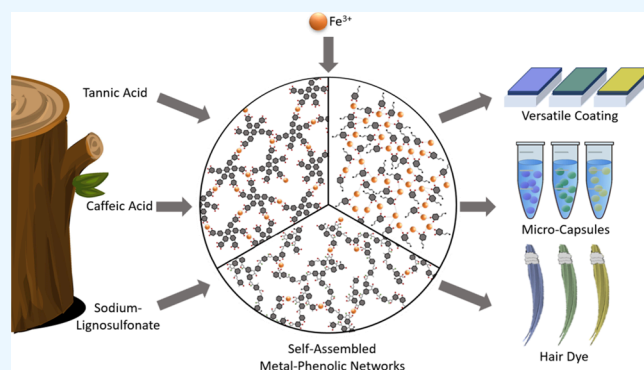
INTRODUCTION

Metal-phenolic networks (MPNs) can be formed by different types of interactions with reversible coordination bonds being expected as the dominant force for MPN formation if transition metals are used.[1] So far, a phenol with at least one vicinal diol group has been deemed essential for the formation of MPN films.[2] We further verified these results by attempting to assemble MPNs from the monolignols coniferyl alcohol, sinapyl alcohol, and *para*-coumaryl alcohol (chemical structure, see Figure 1). MPNs can be used to form empty capsules, which can be used for drug delivery or in MR imaging among others.[3] The reversibility of the coordination bonds offers a chance for disassembly under specific conditions. A change of pH or adding chelating agents like EDTA or reductive agents such as ascorbic acid can be used to selectively disassemble MPNs if needed.[2,4−7] In this research, our aim was to broaden the range of phenols for potential use and conduct comparative analyses with extensively studied tannic acid-Fe^{3+} films. A broad range of phenolic ligands have been used for MPN formation until now, including gallic acid, tannic acid (TA), and epigallocatechin-3-*O*-gallate.[8] We further extended this toolbox of used phenols by utilizing caffeic acid (CaAc) and lignosulfonate (LS). Caffeic acid is a natural polyphenol that occurs in many plants such as coffee, thyme, or sage.[9] Lignosulfonates are easily available as they are a byproduct in the sulfite pulping process. In contrast to lignin, they are water-soluble, which makes them easier to use for MPN formation.[10] LS-Fe^{3+} complexes have been examined for the prevention of iron chlorosis in plants, but not yet for the formation of MPN

films.[11−14] By comparing MPNs made from these new phenols with MPNs formed with tannic acid, we found noticeable differences. They can be disassembled under slightly different conditions and exhibit different colors, opening new fields of use. Previous studies showed the antiviral potential of CaAc-Fe^{3+} complexes, which could be used for antiviral coatings.[15] MPNs made from tannins and iron have already been used as an ink in the European middle ages and for dying teeth black in an old Japanese tradition called "Ohaguro".[16] Furthermore, they were successfully used for hair dying. TA, CaAc, LS, and Fe^{3+} can be considered safe to use on skin for the concentration and amount used in hair dyes.[17−20] The various colors of the MPNs were also used for dyeing human hair.

EXPERIMENTAL SECTION

Materials. All chemicals were used as received, unless stated otherwise. 3-Morpholinopropanesulfonic acid (MOPS) was purchased from Dojindo Laboratories. Tannic acid (TA) was purchased from Merck. Lignosulfonate (LS) and ethyl-enediaminetetraacetic acid disodium salt (EDTA) were purchased from Tokyo Chemical Industry Co. Caffeic acid
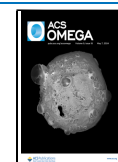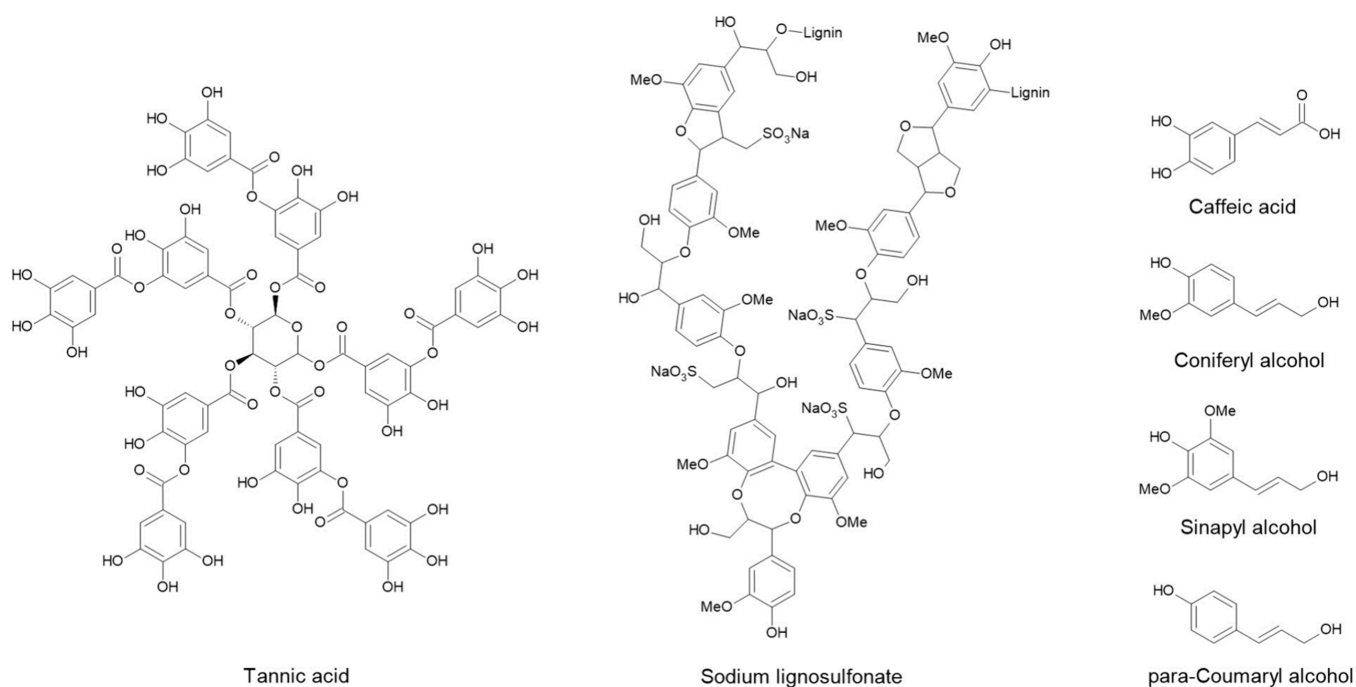
Figure 1. Chemical structures of tannic acid, sodium lignosulfonate, caffeic acid, and the monolignols (coniferyl alcohol, sinapyl alcohol, and *p*-coumaryl alcohol).

(CaAc), iron(III)chloride hexahydrate ($FeCl_3 \cdot 6H_2O$), hydrochloric acid (HCl), sodium hydroxide solution (NaOH, 1 M), (+)-sodium L-ascorbate, ethanol, and tetrahydrofuran (THF) were purchased from Fujifilm Wako Pure Chemicals. Polystyrene (PS) microspheres with a diameter of 3 μm in an aqueous suspension were purchased from Polysciences, Inc. High-purity water (Milli-Q) with a resistivity greater than 18 MΩ cm was obtained from an inline type 1 Merck ultrapure water purification system. For the different experiments, 40 g/L TA solution, 5 g/L CaAc solution (dissolved in 50 wt % ethanol because of poor solubility in water), 10 g/L LS solution, and 10 g/L $FeCl_3 \cdot 6H_2O$ were used to assemble the MPNs.

Instrumentation. UV−vis spectra were recorded by using a Nanodrop One C UV−vis spectrophotometer (Thermo Scientific). To observe the capsules, an Eclipse TE2000-U inverted microscope was used. TEM pictures were obtained using a Jeol JEM-1400 electron microscope by dropping the capsule suspension on a plasma-treated copper grid. The excess liquid was carefully removed by using filter paper. Atomic force microscopy (AFM) images of the capsules were obtained by using a NanoWizard 2 AFM by Bruker. AFM images of the coated glass slides were obtained using a Witec alpha 300 RSA. For contact angle measurements, a contact angle goniometer (SImage Entry 6, Excimer, Inc., Japan) was used, and the pictures were analyzed using a contact angle plugin for ImageJ. Fourier transform infrared (FTIR) spectra were obtained on a Shimadzu IRSpirit spectrometer equipped with an attenuated total reflection accessory (GladiATR, Pike Technologies). To record the X-ray diffraction (XRD) diffractograms, a MiniFlex600/PTN diffractometer was used.

Coating of Cuvettes. In this study, acrylic cuvettes were coated by using the following procedure. The cuvettes were filled with a preset amount of water and a phenolic compound solution. The solution was homogenized for 3 s by using a vortexer. Afterward, a preset amount of $FeCl_3 \cdot 6H_2O$ solution

(10 g/L) was added followed by an additional 3 s homogenization. After each cycle, the solution was removed, and the coating process was repeated. Every fifth cycle, the layer thickness was measured by rinsing and filling the cuvette with water. A UV−vis absorption spectrum ranging from 200 to 850 nm was acquired. For the coating process with TA, the concentrations of TA and Fe^{3+} after mixing were 0.28 and 0.44 mM, respectively. For CaAc, the concentrations of CaAc and Fe^{3+} were 2.6 and 5.3 mM, respectively. For LS, the concentrations of LS and Fe^{3+} were 1 and 0.21 g/L, respectively. The study examined the impact of varying phenol and Fe^{3+} concentrations in the coating solution by halving and doubling them while maintaining a constant phenol-to-Fe^{3+} ratio.

Disassembly Experiments. Precoated cuvettes were employed, showing an absorbance at 320 nm of approximately 0.6, 0.3, and 0.5 for the TA-Fe^{3+}, CaAc-Fe^{3+}, and LS-Fe^{3+} coatings, respectively. HCl was used to adjust the pH to 1 and 4 for the disassembly solutions, while sodium hydroxide was used to achieve pH 12. The pH of the pH 4 solution was monitored daily and adjusted when needed. A buffered 10 mM MOPS solution was utilized for maintaining pH 7.4. The EDTA solution and sodium ascorbate solution had a concentration of 10 mM resulting in pH values of 4.8 and 7.3, respectively. The cuvettes were filled with prepared disassembly solutions. Measurements of the remaining layer thickness were taken at various time intervals. Before the measurement, the disassembly solution was removed, and the cuvette was rinsed with water to remove dissolved components of the MPN coating and filled with fresh disassembly solution. Following the addition of a fresh disassembly solution, a UV−vis absorption spectrum was obtained.

Color of CaAc-Fe^{3+} Complexes. The pH of the CaAc-Fe^{3+} complex was adjusted to observe the impact of the pH change on complex formation. A mixture of water (2 mL), CaAc (25 μL, 27.8 mmol/L), and Fe^{3+} solution (37.5 μL, 37.0
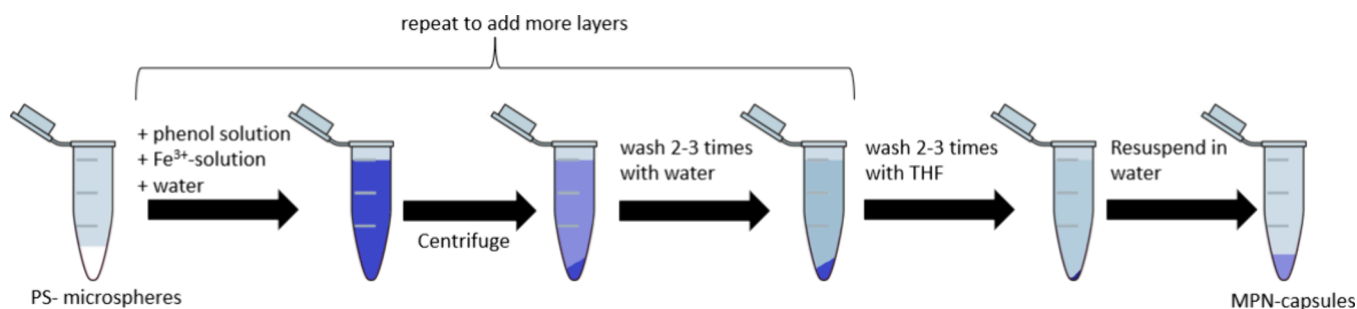
Figure 2. Illustration of the formation of freestanding MPN capsules, including all major steps.
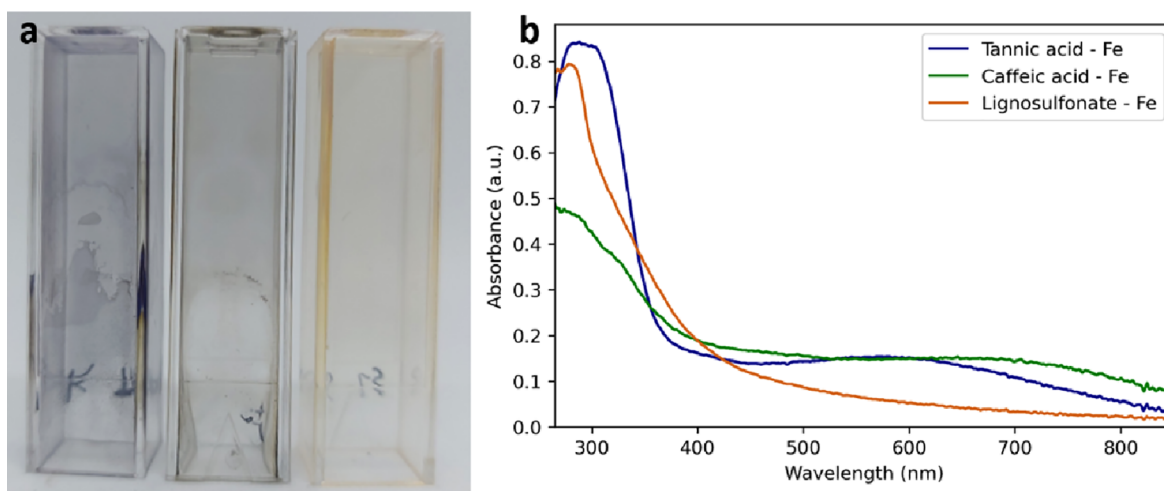
Figure 3. (a) Cuvettes coated with multiple TA-Fe^{3+} (left), CaAc-Fe^{3+} (middle), and LS-Fe^{3+} (right) layers and (b) UV−vis spectra of the coated cuvettes.

mmol/L) was prepared in cuvettes. The pH of the mixtures was adjusted using conc. HCl and NaOH solution (1 mol/L). The pH of the mixtures was incrementally adjusted from pH 1 to pH 11, and UV−vis absorption spectra were measured. After allowing the solution to sit for 3 days, the cuvettes were rinsed with water several times and refilled with water, and UV−vis measurements were conducted to determine at which pH MPN layers were formed.

Formation of MPN Capsules. For the coating of the PS spheres, 50 μL of PS solution was prepared in a centrifuge tube. Preset amounts of water and phenolic compound solution were added and homogenized using a vortexer. FeCl$_3$·6H$_2$O solution (10 g/L) was then added and homogenized for an additional 3 s. The capsules were formed by using the same standard concentrations as those employed for coating the cuvettes. The coated particles were washed by centrifugation (2000g, 2 min), removing the supernatant solution, adding Milli-Q water, and resuspending the particles. This washing step was repeated 3 times with water followed by another 3 washes with THF to dissolve the PS. After removal of the PS, the capsules were resuspended in water. The coating process is illustrated in Figure 2.

Coating Glass Slides. The glass slides were prepared by sonicating and soaking them in water for 20 min. Afterward, they were immersed in ethanol and sonicated for an additional 20 min. The ethanol was then removed, and the glass slides were rinsed with Milli-Q water and air-dried.[21] To coat the glass slides, they were placed in glass vials and subjected to the same coating process as that for the cuvettes. The procedure utilized identical standard concentrations, but the volume of

the coating solution was increased to ensure adequate immersion of the glass slides. After addition of the coating reagents, the solution was allowed to sit for at least 10 min before disposing it and proceeding with the next layer. Three layers were coated on each glass slide for wettability measurements. To reach sufficient thickness of the MPN films for AFM measurements, the coating procedure was carried out 17 times for TA-Fe^{3+} and CaAc-Fe^{3+} and 6 times for LS-Fe^{3+}.

Hair Dyeing. Brunette hair was obtained from a volunteer and bleached with a commercial hair bleaching agent. Following bleaching, the hair was bundled and placed in a centrifuge tube for dyeing. Hair dyeing was performed in the same way as the coating of the glass slides utilizing identical concentrations, except for the TA-Fe^{3+} dyeing procedure, which employed doubled reagent concentrations (0.56 mM TA and 0.89 mM Fe^{3+} in the dyeing solution). The dyeing process was performed either once or thrice to monitor the incremental increase in color intensity with additional dyeing steps.

■ RESULTS AND DISCUSSION

Figure 3a depicts the cuvettes after various coating steps, demonstrating the color change on the cuvette wall. The TA-Fe^{3+} films showed a blue color, while CaAc-Fe^{3+} films were green, and the LS-Fe^{3+} films were orange.

No buffer substance or NaOH was added; hence, the pH of the coating solution remained acidic due to the low pH of the FeCl$_3$·6H$_2$O solution. The TA-Fe^{3+} film showed an absorption band with a maximum at 295 nm as illustrated in Figure 3b. As
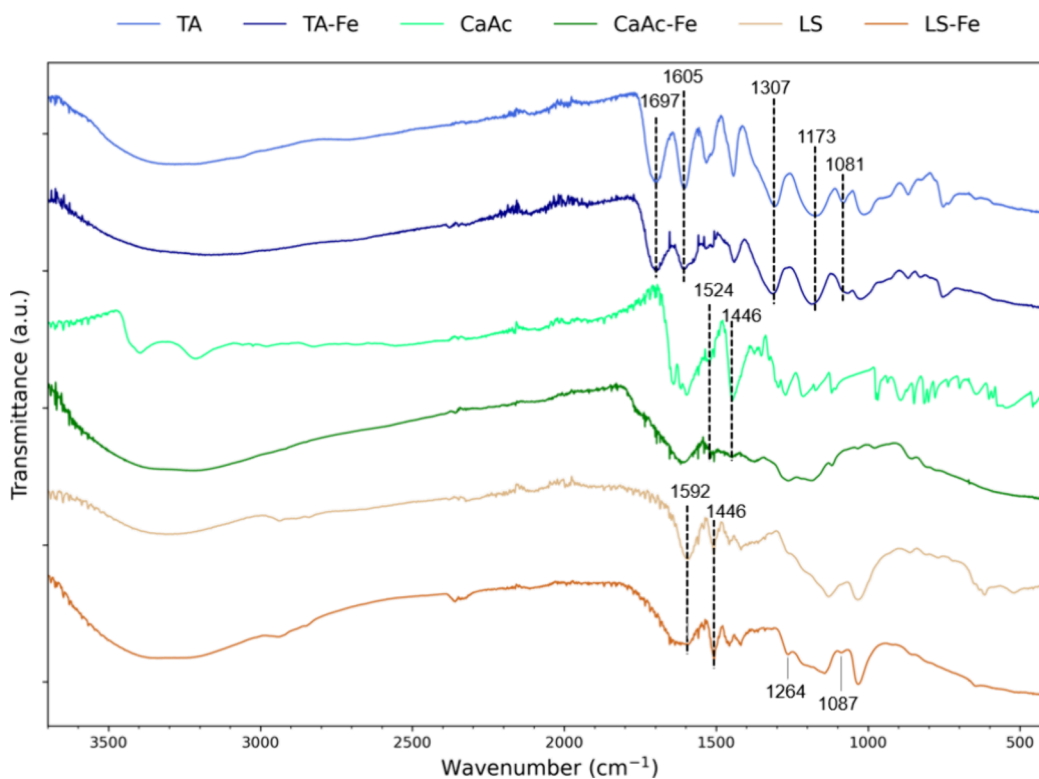
Figure 4. IR spectra of the pure phenols TA, CaAc, and LS and of the MPN complexes (TA-Fe^{3+}, CaAc-Fe^{3+}, and LS-Fe^{3+}).

Figure 5. (a−c) Increase of absorbance at 320 nm after coating with multiple MPN layers with different concentrations of coating reagents. (a) TA-Fe^{3+}, (b) CaAc-Fe^{3+}, and (c) LS-Fe^{3+}. (d−f) Disassembly of the MPN coatings at different conditions. (d) TA-Fe^{3+}, (e) CaAc-Fe^{3+}, and (f) LS-Fe^{3+}.
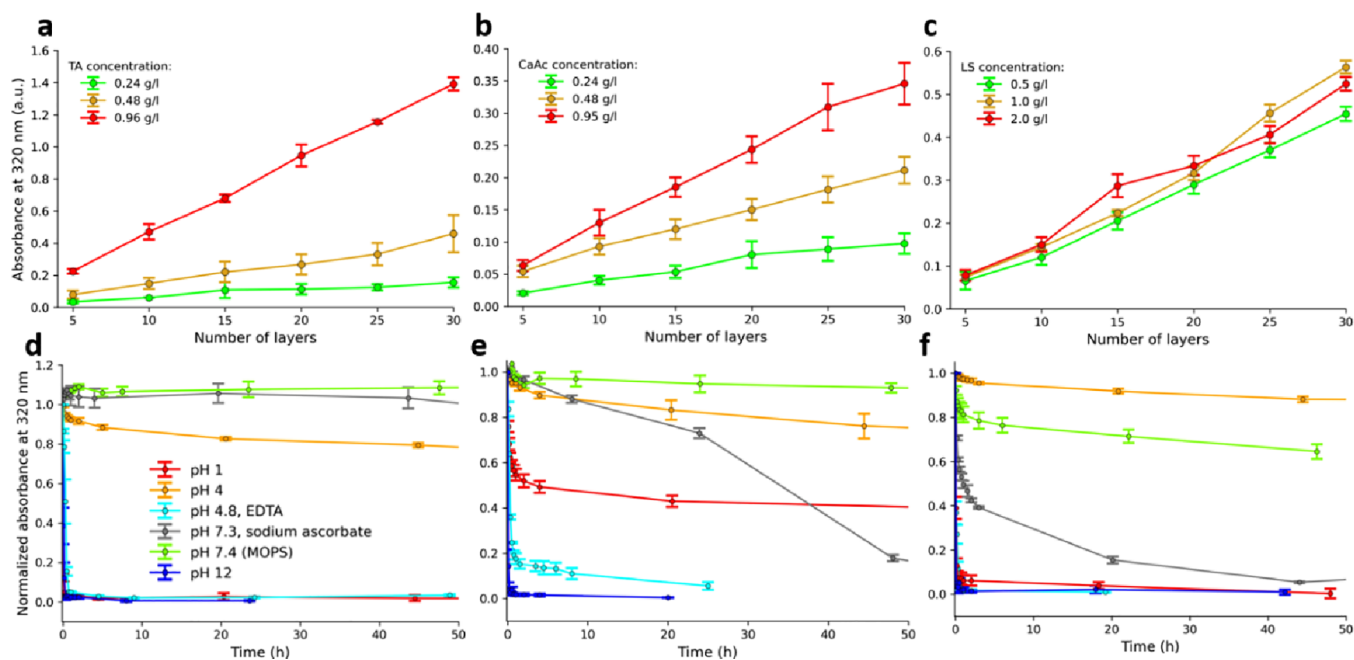
expected, a broad ligand-to-metal charge transfer (LMCT) band at ∼570 nm was observed.[4,22] The CaAc-Fe^{3+} film showed an absorption band with a maximum below 270 nm, exceeding the measurement range accessible with acrylic cuvettes. A broad ligand-to-metal charge transfer band was observed at 650 nm. In contrast to the absorption spectrum of the TA-Fe^{3+} film, the distinction in intensity between the

absorption bands at 280 and 650 nm was reduced, resulting in a more uniform spectrum. The LS-Fe^{3+} film showed one peak at 280 nm, and no LMCT band was observed. It is important to note that except for LS, the pure components exhibit no absorbance above 400 nm (Figure S1).

Figure 4 displays the FTIR spectra of the pure phenolic components alongside those of TA-Fe^{3+}, CaAc-Fe^{3+}, and LS-

Fe^{3+}. The MPNs show a broadening of the absorption band at 3600−3000 cm^{-1}, which is commonly attributed to OH stretching vibrations. This broadening may result from the formation of coordination bonds between the OH groups and Fe^{3+} or from residual moisture within the MPNs.[23,24]

TA shows a broad absorption band at 3260 cm^{-1}, which can be attributed to OH stretching vibrations. Some other characteristic bands appear at 1697 (C=O stretching), 1605 (C−C stretching of aromatics), 1307 (C−O−C stretching of aromatics with contributions of C−O−H in-plane bending of the phenol and C−C stretching of aromatics), 1173 (stretching vibrations of the ester and in-plane bending of phenol), and 1081 cm^{-1} (C−O stretching of phenols).[25,26] Compared to TA, the bands at 1307, 1173, and 1081 shifted to 1316, 1182, and 1067 cm^{-1}, in TA-Fe^{3+}, respectively, indicating interactions between Fe^{3+} and the phenolic hydroxyl group.[27,28]

In the spectrum of CaAc, two bands corresponding to the OH stretching vibrations were visible at 3398 and 3216 cm^{-1}. The bands at 1524 and 1446 cm^{-1} correspond to C−C stretching vibrations of the aromatic ring. For the spectrum of CaAc-Fe^{3+}, the bands were less sharp, the intensity of many bands decreased, band positions shifted, and some small bands became more distinctive.[29,30]

The spectrum of LS shows a broad absorption band at 3311 cm^{-1} caused by OH stretching vibrations as well as bands corresponding to C−H stretching vibrations around 2900 cm^{-1}. The bands at 1592 and 1508 cm^{-1} can be associated with vibrations of the aromatic rings in LS. LS-Fe^{3+} exhibited considerable broadening of the band at 1592 cm^{-1}, along with the emergence of new bands at 1264 and 1087 cm^{-1}.[31]

The XRD diffractograms for both TA and TA-Fe^{3+} indicate an amorphous structure (see Figure S2a), which is consistent with previous findings.[2] In contrast to that, the diffractograms of LS-Fe^{3+} and CaAc-Fe^{3+} show more and sharper reflexes than the pure phenols, suggesting that they are at least partially crystalline (Figure S2b,c).[32]

The multiple layer coating experiments showed a linear dependence between the absorbance of the MPN coatings and the number of layers. A strong concentration dependence was observed for the TA-Fe^{3+} film buildup within the coating solution's concentration range of 0.24 to 0.96 g/L TA (Figure 5a). Higher concentrations were examined, but the absorbance limit for the UV−vis measurement was exceeded quickly. The CaAc-Fe^{3+} film buildup was examined in the same concentration range. A direct proportional relationship between the buildup and the concentration was observed (Figure 5b). The LS-Fe^{3+} film buildup exhibited almost no concentration dependence for LS concentrations ranging from 0.5 to 2 g/L in the coating solution (Figure 5c).

The disassembly experiments revealed that neither of the films was stable at high and low pH values (Figure 5, bottom, close up of the first 2 h, and Figure S3). For the CaAc-Fe^{3+} films, only partial disassembly seemed to occur at pH 1. The LMCT band at 650 nm disappeared completely, while part of the absorbance at smaller wavelengths remained. EDTA disassembled all films, suggesting their breakdown through competitive chelation. This validates the assumption of layer formation through the coordinative interaction between phenols and Fe^{3+}. The TA-Fe^{3+} films and CaAc-Fe^{3+} films were stable at neutral pH, but for TA-Fe^{3+}, a change in the absorption spectrum was observed. The maximum shifted to 310 nm, and the broad LMCT band was shifted to slightly shorter wavelengths around 560 nm (Figure S4). The color of

the layer changed slightly to purple, which is in accordance with the color found for TA-Fe^{3+} complexes at pH 7.[4] Unexpectedly, LS-Fe^{3+} films were not stable in MOPS solution, and after approximately 1 h, 20% of the coating was degraded. Conversely, the film exhibited high stability at pH 4, with less than 13% of the coating degraded after 68 h. The TA-Fe^{3+} films and CaAc-Fe^{3+} films were less stable at pH 4; after 68 h, 74 and 73% of the intensity at 320 nm remained, respectively. In sodium ascorbate solution, the TA-Fe^{3+} films did not seem to disassemble at first. However, after 68 h, the layers started to show signs of degradation. In two of three attempts, after 91 h, 37 and 41% of the intensity at 320 nm remained, while for the third attempt, 81% of the intensity remained. Seemingly, the degradation started later in that attempt. The CaAc-Fe^{3+} films started to disassemble earlier, with slow degradation in the beginning and then faster degradation after 24 h. The LS-Fe^{3+} film showed typical degradation behavior, and the absorbance at 320 nm was reduced by 95% after 44 h. The different disassembly behavior of the LS-Fe^{3+} films may be caused by different functional groups in LS associated with complex formation, including carboxyl, hydroxyl, and sulfonate groups.[13,33]

The color of the CaAc-Fe^{3+} complex was strongly pH-dependent. At pH 1, the complex appeared almost colorless with a slight yellow tone (Figure 6a). At pH 3 and 4, the
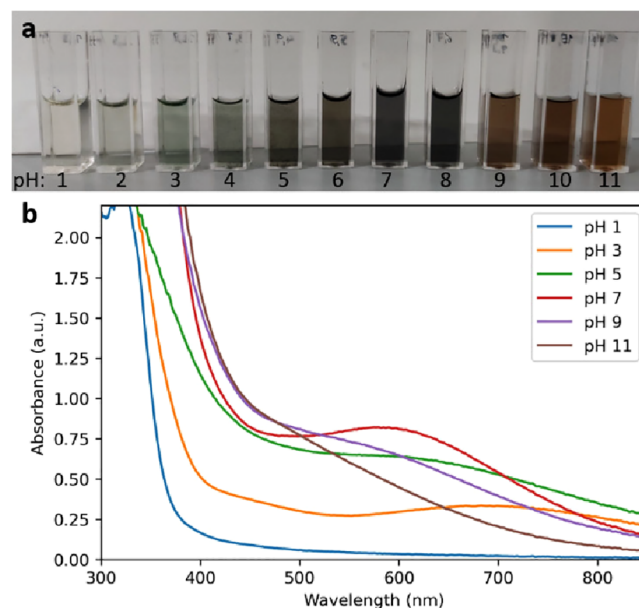
Figure 6. (a) Color of the CaAc-Fe complex at different pH. (b) UV−vis spectra of the complex at different pH.

complex was green, shifting to green gray at a pH of 5−6. At pH 7 and 8, the solution was gray, while at a pH of 9 and above, the solution was brown red. The color change can be expected to occur due to the transition between mono, bis, and tris complexes. The change between the different complex types influences the location of the LMCT band as well. The LMCT band appeared at 700 nm at pH 3 and shifted to 600 nm at pH 7 (Figure 6b). These pH-dependent changes in the color and coordination state of the complex are similar to the behavior reported for TA-Fe^{3+} and catechol-Fe^{3+} complexes.[4,34−36] The UV−vis absorption spectra at pH 9 were in accordance with CaAc-Fe spectra found in the literature.[29] Precipitation was visible within 3 days across a pH range of 3

to 6 (Figure S5a). Layer formation with absorbance at wavelengths above 450 nm could be observed from pH 3 to 8 (Figure S5b). At higher pH, no layer formation at the cuvette walls was observed, and at lower pH values, absorbance could only be observed at smaller wavelengths. The absence of layer buildup at high pH might result from the oxidation of CaAc at basic conditions rendering it incapable to form complexes.[37]

Several observations during capsule production aid in predicting the process success. After adding the phenol and Fe^{3+} solution, complex formation should occur, resulting in a change in the color of the solution (Figure 7a). After the
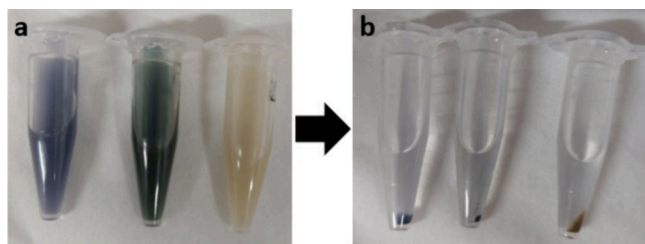
Figure 7. (a) PS microsphere solution after combination with TA-Fe^{3+} (blue), CaAc-Fe^{3+} (green), and LS-Fe^{3+} (straw). (b) After dissolving the PS and centrifugation, the hollow capsules remain.

sample was washed, the changed color of the remaining coated PS microspheres should be apparent. Hollow capsules remain visible at the bottom of the centrifuge tube after dissolving the PS scaffold and subsequent centrifugation (Figure 7b).

Capsules were successfully formed using TA, CaAc, and LS (Figure 8). The TA-Fe^{3+} and CaAc-Fe^{3+} capsules exhibited a smooth surface, with only a minority of the capsules broken (Figure 8a,b). Optical microscopy of the suspended capsules showed that the surface of the LS-Fe^{3+} capsules was rough and uneven, and many of the capsules were damaged. TEM images depict debris attached to the LS-Fe^{3+} capsules (Figure 8c). A

factor that generally proved to be crucial for capsule formation was the phenol:Fe^{3+} ratio. Initially, an attempted mass ratio of 19.4:1 for LS-Fe^{3+} failed to yield any capsules. After the mass ratio was changed to 4.84:1, capsule formation succeeded. For CaAc-Fe^{3+}, a molar ratio of 3:2 was tried, but the formation of capsules failed. Capsules formed successfully at a molar ratio of 1:2. For TA-Fe^{3+}, a molar ratio of 1:1.6 was used successfully, as suggested in the literature.[4,22]

AFM pictures of the capsules were obtained (Figure 9). The thickness of the capsules was determined by using line profiles. The TA-Fe^{3+}, CaAc-Fe^{3+}, and LS-Fe^{3+} capsule thicknesses were found to be 12 ± 4, 21 ± 6, and 23 ± 3 nm, respectively. Consequently, the estimated single-layer thicknesses, presumed to be half the capsule thickness, were 6 ± 2, 11 ± 3, and 11 ± 2 nm. In accordance with previous results, the LS-Fe^{3+} capsules exhibited an attached precipitate (see Figure 9b).

The glass slides coated with TA-Fe^{3+}, CaAc-Fe^{3+}, and LS-Fe^{3+} show blue, green, and straw colors, respectively (Figure S6). In contrast to the single-layer thickness of the capsules, the single-layer thickness on the glass slides was much smaller, suggesting a lower capability of the MPNs to coat the glass surface. AFM images of the MPN layer can be found in the Supporting Information (Figure S7, top). For 17 layers of TA-Fe^{3+} and CaAc-Fe^{3+} and 6 layers of LS-Fe^{3+}, the total thicknesses calculated from the line profiles (Figure S7, bottom) were 31 ± 2, 17 ± 1, and 21 ± 2 nm, respectively. They correspond to single-layer thicknesses of 1.8 ± 0.1, 1.0 ± 0.1, and 3.4 ± 0.3 nm for TA-Fe^{3+}, CaAc-Fe^{3+}, and LS-Fe^{3+} accordingly.

Following washing, the contact angle of water on the glass slide was measured to be $26 \pm 7°$ (Figure 10). The MPN coating increased the contact angle considerably. TA-Fe^{3+} and CaAc-Fe^{3+} coatings showed similar wettability with contact angles of 44 ± 6 and $50 \pm 5°$, respectively. Conversely, the LS-Fe^{3+} coating had the lowest wettability, with a contact angle of $81 \pm 3°$. A significant influence of the choice of ligand on the
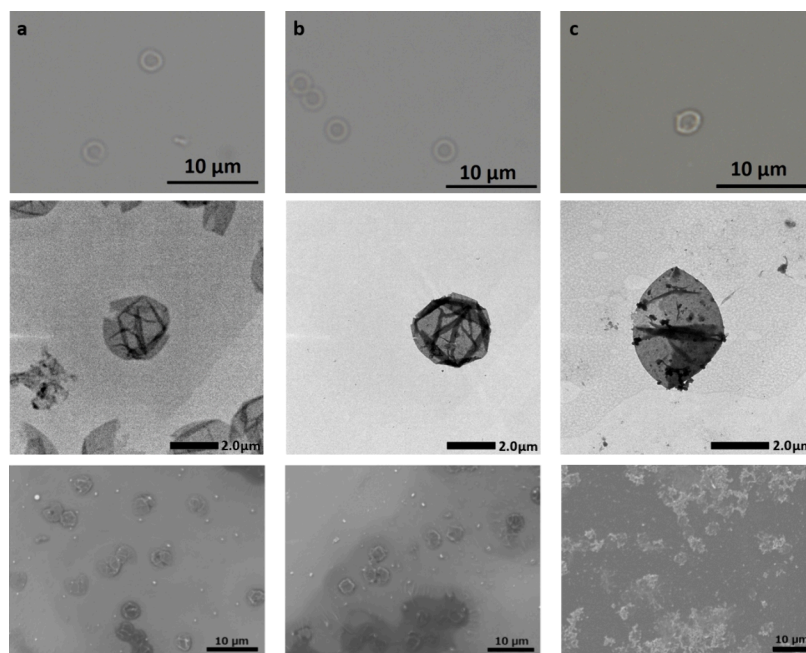
Figure 8. Images of the MPN capsules obtained using optical microscopy, SEM, and TEM (top to bottom, respectively). (a) TA-Fe^{3+}, (b) CaAc-Fe^{3+}, and (c) LS-Fe^{3+}.
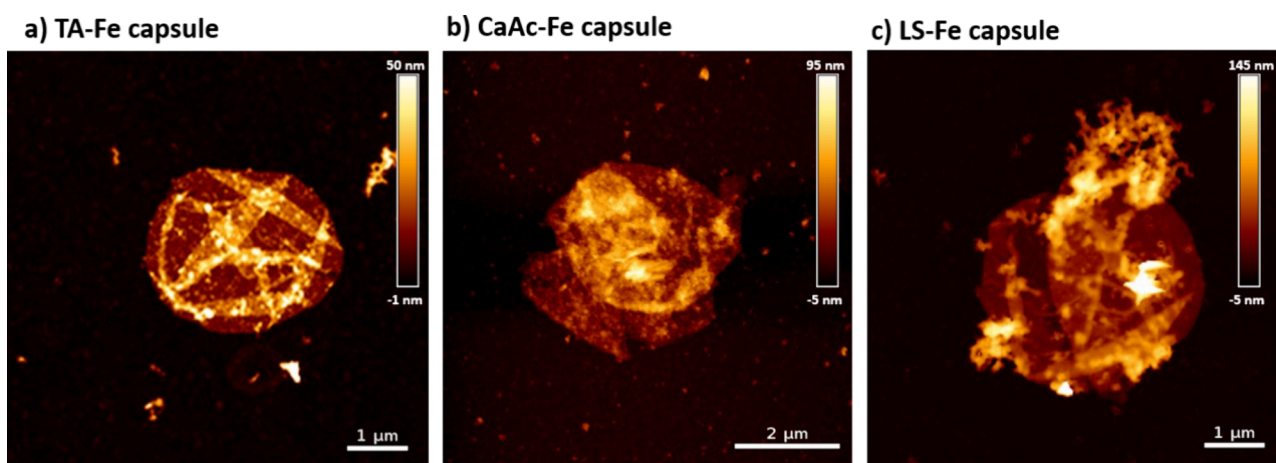
Figure 9. AFM pictures of (a) TA-Fe^{3+}, (b) CaAc-Fe^{3+}, and (c) LS-Fe^{3+} capsules.
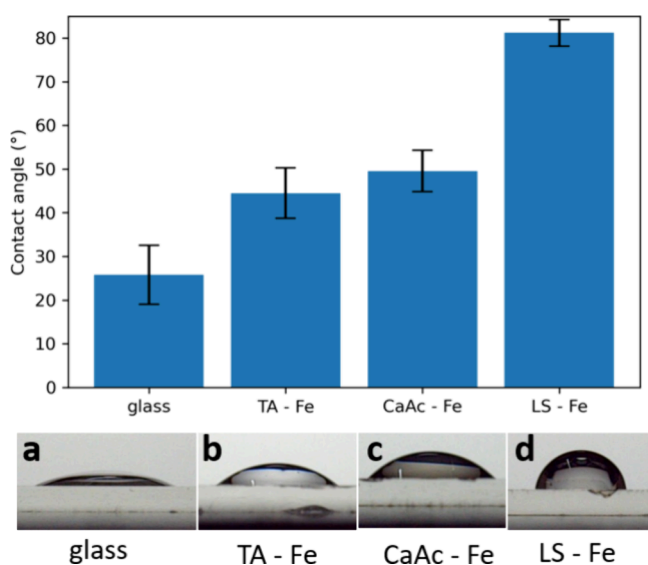
Figure 10. Water contact angles of (a) glass and glass coated with (b) TA-Fe^{3+}, (c) CaAc-Fe^{3+}, and (d) LS-Fe^{3+} coatings.

contact angle was shown by Yun et al.[22] They hypothesized that the different capability of the films to form hydrogen bonds might be the underlying cause.

Human hair was dyed in different colors, depending on the type of MPN used. The TA-Fe^{3+}-dyed hair was blue-purple, but the coating's uneven attachment led to irregular color distribution (Figure 11a). Hair dyed with CaAc-Fe^{3+} exhibited an emerald-green color (Figure 11b). LS-Fe^{3+} dyed the hair a straw-yellow color (Figure 11c). The color of the dyed hair, as well as the intensification of the color with additional layers, agrees with the previously discussed results. The prior bleaching step was important, as the intensity of the hair dye was not strong enough to cover the originally brunette color of the used human hair (Figure S8). For enhancing the dyeing process, the strategy of premixing metal and phenol solutions followed by precipitate removal through centrifugation to obtain ready-to-use dyeing solutions, as suggested by Geng et al.,[21] could be beneficial. In situ oxidation of Fe^{2+} to Fe^{3+} may also help to improve the process.[38,39]

Efforts to form MPN films using *p*-coumaryl alcohol, coniferyl alcohol, and sinapyl alcohol showed no successful buildup for coniferyl alcohol and sinapyl alcohol. Slight MPN

Figure 11. Strands of hair dyed using (a) TA-Fe^{3+}, (b) CaAc-Fe^{3+}, and (c) LS-Fe^{3+} coatings. The left hair strand on each image shows the bleached hair, and the middle and right hair strands were dyed once and thrice, respectively.

formation tendencies were observed with *p*-coumaryl alcohol. A weak LMCT band appeared at 600 nm in the UV–vis spectrum when combining *p*-coumaryl alcohol and Fe solution (Figure S9b). It was further verified by introducing *p*-coumaryl alcohol solution (1 g/L) buffered to pH 7.4 using MOPS into a cuvette, leaving it undisturbed for roughly 10 min. Subsequently, the cuvette was rinsed with water before adding $FeCl_3 \cdot 6H_2O$ solution (1 g/L), which also was left to age for approximately 10 min. The cuvette was rinsed with water again, and this alternating sequence was repeated multiple times. However, the standard coating process and the formation of capsules failed because rather than forming a continuous coating, the *p*-coumaryl alcohol-Fe formed stains on the cuvette walls (Figure S9a). The failed formation of MPNs can be explained by the lack of vicinal hydroxyl groups in the structure of the monolignols. CaAc and TA possess vicinal hydroxyl groups, while lignosulfonate has a multitude of other functional groups, which may bind to metals.[40]

CONCLUSIONS

In summary, the successful formation of MPNs with Fe^{3+} using CaAc and LS was verified, and the properties of the new MPNs were compared with TA-Fe^{3+} MPNs. The assembly was simple and fast and worked on various surfaces, resulting in the formation of thin layers on the nanometer scale. Their different characteristics make them suitable candidates for a wide range of applications. As an example, their potential as a dye for human hair has been successfully demonstrated.

In the future, the properties of the MPNs could be further tuned by using different metal ions or derivatizing CaAc. We expect the MPNs to exhibit antibacterial properties due to the antibacterial traits of CaAc and LS, which could be useful for various applications in medical fields.[15,41,42] Maybe the Fe^{3+} in the MPNs can be partially reduced by the phenols and mediate the Fenton reaction, which is known to exhibit antibacterial effects.[43,44] However, further research is needed to prove this assumption.

ASSOCIATED CONTENT

Ⓢ Supporting Information

The Supporting Information is available free of charge at https://pubs.acs.org/doi/10.1021/acsomega.4c01399.

UV–vis spectra of phenols and Fe^{3+}; XRD diffractograms of TA, TA-Fe^{3+}, CaAc, CaAc-Fe^{3+}, LS, and LS-Fe^{3+}; disassembly graph of TA-Fe^{3+}, CaAc-Fe^{3+}, and LS-Fe^{3+} for the first 2 h; UV–vis spectrum of the TA-Fe^{3+} coating in an MOPS buffer; picture of the CaAc-Fe^{3+} complex at different pH after 3 days and UV–vis spectra of the formed coating; images of MPN-coated glass slides; AFM images of MPN-coated glass slides; images of the brunette human hair coated with CaAc-Fe^{3+}, *p*-coumaryl alcohol-Fe^{3+}-coated cuvette, and corresponding UV–vis spectrum (PDF)

AUTHOR INFORMATION

Corresponding Author

Daniela Tomasetig − *Department of Materials Engineering, School of Engineering, The University of Tokyo, Tokyo 113-8656, Japan; Institute of Chemical Technologies and Analytics, TU Wien, Vienna 1060, Austria;* ⓘ orcid.org/0009-0004-2779-6384; Email: daniela.tomasetig@tuwien.ac.at

Authors

Chenyu Wang − *Department of Materials Engineering, School of Engineering, The University of Tokyo, Tokyo 113-8656, Japan;* ⓘ orcid.org/0000-0001-7035-6924

Nikolaus Hondl − *Institute of Chemical Technologies and Analytics, TU Wien, Vienna 1060, Austria;* ⓘ orcid.org/0009-0001-9282-4474

Anton Friedl − *Institute of Chemical, Environmental and Bioscience Engineering, TU Wien, Vienna 1060, Austria;* ⓘ orcid.org/0000-0002-0450-9707

Hirotaka Ejima − *Department of Materials Engineering, School of Engineering, The University of Tokyo, Tokyo 113-8656, Japan;* ⓘ orcid.org/0000-0002-4965-9493

Complete contact information is available at: https://pubs.acs.org/10.1021/acsomega.4c01399

Author Contributions

The manuscript was written through contributions of all authors. All authors have given approval to the final version of the manuscript.

Notes

The authors declare no competing financial interest.

ABBREVIATIONS

AFM atomic force microscopy,; EDTA ethylenediaminetetraacetic acid; CaAc caffeic acid; LS lignosulfonate; MOPS 3-morpholinopropanesulfonic acid; MPNs metal-phenolic networks; TA tannic acid; XRD X-ray diffraction

REFERENCES

(1) Guo, J.; Ping, Y.; Ejima, H.; Alt, K.; Meissner, M.; Richardson, J. J.; Yan, Y.; Peter, K.; von Elverfeldt, D.; Hagemeyer, C. E.; Caruso, F. Engineering Multifunctional Capsules through the Assembly of Metal−Phenolic Networks. *Angew. Chem., Int. Ed.* **2014**, *53* (22), 5546−5551.

(2) Rahim, Md. A.; Kempe, K.; Müllner, M.; Ejima, H.; Ju, Y.; van Koeverden, M. P.; Suma, T.; Braunger, J. A.; Leeming, M. G.; Abrahams, B. F.; Caruso, F. Surface-Confined Amorphous Films from Metal-Coordinated Simple Phenolic Ligands. *Chem. Mater.* **2015**, *27* (16), 5825−5832.

(3) Dai, Q.; Geng, H.; Yu, Q.; Hao, J.; Cui, J. Polyphenol-Based Particles for Theranostics. *Theranostics* **2019**, *9* (11), 3170−3190.

(4) Ejima, H.; Richardson, J. J.; Liang, K.; Best, J. P.; Van Koeverden, M. P.; Such, G. K.; Cui, J.; Caruso, F. One-Step Assembly of Coordination Complexes for Versatile Film and Particle Engineering. *Science* **2013**, *341* (6142), 154−157.

(5) Rahim, Md. A.; Björnmalm, M.; Bertleff-Zieschang, N.; Ju, Y.; Mettu, S.; Leeming, M. G.; Caruso, F. Multiligand Metal−Phenolic Assembly from Green Tea Infusions. *ACS Appl. Mater. Interfaces* **2018**, *10* (9), 7632−7639.

(6) Park, J. H.; Kim, K.; Lee, J.; Choi, J. Y.; Hong, D.; Yang, S. H.; Caruso, F.; Lee, Y.; Choi, I. S. A Cytoprotective and Degradable Metal-Polyphenol Nanoshell for Single-Cell Encapsulation. *Angew. Chem., Int. Ed.* **2014**, 12628−12633.

(7) Lee, H.; Park, J.; Han, S. Y.; Han, S.; Youn, W.; Choi, H.; Yun, G.; Choi, I. S. Ascorbic Acid-Mediated Reductive Disassembly of Fe

[3+]-Tannic Acid Shells in Degradable Single-Cell Nanoencapsulation. *Chem. Commun.* **2020**, *56* (89), 13748−13751.

(8) Geng, H.; Zhong, Q.-Z.; Li, J.; Lin, Z.; Cui, J.; Caruso, F.; Hao, J. Metal Ion-Directed Functional Metal−Phenolic Materials. *Chem. Rev.* **2022**, *122* (13), 11432−11473.

(9) *Bioactive Natural Products*; Atta-ur-Rahman, Ed.; Studies in natural products chemistry; MA Elsevier: Amsterdam Oxford Cambridge, 2022.

(10) Niaounakis, M.Biopolymers: Applications and Trends; *Plastics design library series*; Elsevier: Amsterdam, 2015.

(11) Carrasco, J.; Kovács, K.; Czech, V.; Fodor, F.; Lucena, J. J.; Vértes, A.; Hernández-Apaolaza, L. Influence of pH, Iron Source, and Fe/Ligand Ratio on Iron Speciation in Lignosulfonate Complexes Studied Using Mössbauer Spectroscopy. Implications on Their Fertilizer Properties. *J. Agric. Food Chem.* **2012**, *60* (13), 3331−3340.

(12) Rodríguez-Lucena, P.; Lucena, J. J.; Hernández-Apaolaza, L.*Relationship between the Structure of Fe-Lignosulfonate Complexes Determined by FTIR Spectroscopy and Their Reduction by the Leaf Fe Reductase*. 2009.

(13) Khabarov, Yu. G.; Veshnyakov, V. A.; Shergin, A. E. Electrochemical Synthesis and Biological Activity of Iron Lignosulfonate. *Russ Chem. Bull.* **2019**, *68* (5), 1081−1087.

(14) Rodríguez-Lucena, P.; Benedicto, A.; Lucena, J. J.; Rodríguez-Castrillón, J. A.; Moldovan, M.; García Alonso, J. I.; Hernández-Apaolaza, L. Use of the Stable Isotope [57]Fe to Track the Efficacy of the Foliar Application of Lignosulfonate/Fe [3+] Complexes to Correct Fe Deficiencies in Cucumber Plants: Lignosulfonate/ [57] Fe [3+] Complexes to Correct Fe Chlorosis. *J. Sci. Food Agric.* **2011**, *91* (3), 395−404.

(15) Langland, J.; Jacobs, B.; Wagner, C. E.; Ruiz, G.; Cahill, T. M. Antiviral Activity of Metal Chelates of Caffeic Acid and Similar Compounds towards Herpes Simplex, VSV-Ebola Pseudotyped and Vaccinia Viruses. *Antiviral Res.* **2018**, *160*, 143−150.

(16) Venugopal, A.; Marya, A. Return of the Ohaguro. *Br Dent J.* **2021**, *231* (2), 69−69.

(17) Nakamura, T.; Yoshida, N.; Yasoshima, M.; Kojima, Y. Effect of Tannic Acid on Skin Barrier Function. *Experimental Dermatology* **2018**, *27* (8), 824−826.

(18) Spagnol, C. M.; Di Filippo, L. D.; Isaac, V. L. B.; Correa, M. A.; Salgado, H. R. N. Caffeic Acid in Dermatological Formulations: In Vitro Release Profile and Skin Absorption. *CCHTS* **2017**, *20* (8), 675 DOI: 10.2174/1386207320666170602090448.

(19) Schrenk, D.; Bignami, M.; Bodin, L.; Chipman, J. K.; del Mazo, J.; Grasl-Kraupp, B.; Hogstrand, C.; Hoogenboom, L.; Leblanc, J.; Nebbia, C. S.; Nielsen, E.; Ntzani, E.; Petersen, A.; Sand, S.; Schwerdtle, T.; Wallace, H.; Grob, K.; Castle, L.; Christodoulidou, A.; Vleminckx, C. Evaluation of Calcium Lignosulfonate as a Acceptable Previous Cargo for Edible Fats and Oils. *EFS2* **2019**, *17* (12), e05951 DOI: 10.2903/j.efsa.2019.5951. EFSA Panel on Contaminants in the Food Chain (CONTAM);

(20) Loewit, K.; Födisch, H.-J.; Zambelis, N.; Egg, D. Contraceptive Effect of Iron: Local Compatibility of Vaginally Applied Iron in Rats and Mice. *Contraception* **1972**, *6* (1), 65−70.

(21) Geng, H.; Zhuang, L.; Li, M.; Liu, H.; Caruso, F.; Hao, J.; Cui, J. Interfacial Assembly of Metal−Phenolic Networks for Hair Dyeing. *ACS Appl. Mater. Interfaces* **2020**, *12*, 29826.

(22) Yun, G.; Besford, Q. A.; Johnston, S. T.; Richardson, J. J.; Pan, S.; Biviano, M.; Caruso, F. Self-Assembly of Nano- to Macroscopic Metal−Phenolic Materials. *Chem. Mater.* **2018**, *30* (16), 5750−5758.

(23) Lin, Z.; Zhou, J.; Cortez-Jugo, C.; Han, Y.; Ma, Y.; Pan, S.; Hanssen, E.; Richardson, J. J.; Caruso, F. Ordered Mesoporous Metal−Phenolic Network Particles. *J. Am. Chem. Soc.* **2020**, *142* (1), 335−341.

(24) Li, Y. M.; Miao, X.; Wei, Z. G.; Cui, J.; Li, S. Y.; Han, R.; Zhang, Y.; Wei, W. Iron-Tannic Acid Nanocomplexes: Facile Synthesis and Application for Removal of Methylene Blue from Aqueous Solution. *Dig. J. Nanomater. Biostructures* **2016**, *11*, 1045−1061.

(25) Socrates, G.*Infrared and Raman Characteristic Group Frequencies: Tables and Charts*, 3. ed., repr. as paperback.; Wiley: Chichester, 2010.

(26) Ranoszek-Soliwoda, K.; Tomaszewska, E.; Socha, E.; Krzyczmonik, P.; Ignaczak, A.; Orlowski, P.; Krzyzowska, M.; Celichowski, G.; Grobelny, J. The Role of Tannic Acid and Sodium Citrate in the Synthesis of Silver Nanoparticles. *J. Nanopart. Res.* **2017**, *19* (8), 273.

(27) Wang, W.; Wang, H.; Zhao, J.; Wang, X.; Xiong, C.; Song, L.; Ding, R.; Han, P.; Li, W. Self-Healing Performance and Corrosion Resistance of Graphene Oxide−Mesoporous Silicon Layer−Nanosphere Structure Coating under Marine Alternating Hydrostatic Pressure. *Chemical Engineering Journal* **2019**, *361*, 792−804.

(28) Zhang, R.; Li, L.; Liu, J. Synthesis and Characterization of Ferric Tannate as a Novel Porous Adsorptive-Catalyst for Nitrogen Removal from Wastewater. *RSC Adv.* **2015**, *5* (51), 40785−40791.

(29) Singh, K.; Kumar, A. Kinetics of Complex Formation of Fe(III) with Caffeic Acid: Experimental and Theoretical Study. *Spectrochimica Acta Part A: Molecular and Biomolecular Spectroscopy* **2019**, *211*, 148−153.

(30) Zhou, Q.; Yan, B.; Xing, T.; Chen, G. Fabrication of Superhydrophobic Caffeic Acid/Fe@cotton Fabric and Its Oil-Water Separation Performance. *Carbohydr. Polym.* **2019**, *203*, 1−9.

(31) Boeriu, C. G.; Bravo, D.; Gosselink, R. J. A.; Van Dam, J. E. G. Characterisation of Structure-Dependent Functional Properties of Lignin with Infrared Spectroscopy. *Industrial Crops and Products* **2004**, *20* (2), 205−218.

(32) Ghodke, S. A.; Maheshwari, U.; Gupta, S.; Sonawane, S. H.; Bhanvase, B. A.Nanomaterials for Adsorption of Pollutants and Heavy Metals: Introduction, Mechanism, and Challenges. In *Handbook of Nanomaterials for Wastewater Treatment*; Elsevier, 2021; pp 343−366. DOI: 10.1016/B978-0-12-821496-1.00032-5.

(33) Merdy, P.; Guillon, E.; Frapart, Y.-M.; Aplincourt, M. Iron and Manganese Surface Complex Formation with Extracted Lignin. Part 2: Characterisation of Magnetic Interaction between Transition Metal and Quinonic Radical by EPR Microwave Power Saturation Experiments. *New J. Chem.* **2003**, *27* (3), 577−582.

(34) Xu, H.; Nishida, J.; Ma, W.; Wu, H.; Kobayashi, M.; Otsuka, H.; Takahara, A. Competition between Oxidation and Coordination in Cross-Linking of Polystyrene Copolymer Containing Catechol Groups. *ACS Macro Lett.* **2012**, *1* (4), 457−460.

(35) Sever, M. J.; Wilker, J. J. Visible Absorption Spectra of Metal−Catecholate and Metal−Tironate Complexes. *Dalton Trans.* **2004**, *7*, 1061−1072.

(36) Hynes, M. J.; O'Coinceanainn, M. The Kinetics and Mechanisms of Reactions of Iron(III) with Caffeic Acid, Chlorogenic Acid, Sinapic Acid, Ferulic Acid and Naringin☆. *Journal of Inorganic Biochemistry* **2004**, *98* (8), 1457−1464.

(37) Friedman, M.; Jürgens, H. S. Effect of pH on the Stability of Plant Phenolic Compounds. *J. Agric. Food Chem.* **2000**, *48* (6), 2101−2110.

(38) Han, S.; Hong, S.-P.; Kang, E.; Kim, B.; Lee, H.; Kim, W.; Choi, I. Iron Gall Ink Revisited: Natural Formulation for Black Hair-Dyeing. *Cosmetics* **2019**, *6* (2), 23.

(39) Han, S. Y.; Kang, E. K.; Choi, I. S. Iron Gall Ink Revisited: A Surfactant-Free Emulsion Technology for Black Hair-Dyeing Formulation. *Cosmetics* **2021**, *8* (1), 9.

(40) Fedenko, V. S.; Landi, M.; Shemet, S. A. Metallophenolomics: A Novel Integrated Approach to Study Complexation of Plant Phenolics with Metal/Metalloid Ions. *IJMS* **2022**, *23* (19), 11370.

(41) Chen, M.; Li, Y.; Liu, H.; Zhang, D.; Shi, Q.-S.; Zhong, X.-Q.; Guo, Y.; Xie, X.-B. High Value Valorization of Lignin as Environmental Benign Antimicrobial. *Materials Today Bio* **2023**, *18*, No. 100520.

(42) Zhang, Z.; Wang, D.; Qiao, S.; Wu, X.; Cao, S.; Wang, L.; Su, X.; Li, L. Metabolic and Microbial Signatures in Rat Hepatocellular Carcinoma Treated with Caffeic Acid and Chlorogenic Acid. *Sci. Rep* **2017**, *7* (1), 4508.

(43) Wang, D.; Xing, J.; Zhang, Y.; Guo, Z.; Deng, S.; Guan, Z.; He, B.; Ma, R.; Leng, X.; Dong, K.; Dong, Y. Metal−Phenolic Networks for Chronic Wounds Therapy. *IJN* **2023**, *18*, 6425−6448.

(44) Xu, Y.; Xiao, L.; Chen, J.; Wu, Q.; Yu, W.; Zeng, W.; Shi, Y.; Lu, Y.; Liu, Y. α-Fe2O3 Based Nanotherapeutics for near-Infrared/ Dihydroartemisinin Dual-Augmented Chemodynamic Antibacterial Therapy. *Acta Biomaterialia* **2022**, *150*, 367−379.